ACS OMEGA

Open Access

http://pubs.acs.org/journal/acsodf

Article

A Model System of Biocompatible Organic–Inorganic Materials Containing Salicylate Peptides and Calcite: Insights into Precipitation Kinetics

Lara Jurković, Andreja Jakas, Matija Gredičak, and Damir Kralj*

Cite This: *ACS Omega* 2026, 11, 14002−14016

Read Online

ACCESS | Metrics & More | Article Recommendations | Supporting Information

ABSTRACT: Biomaterials and their formation processes in living organisms (biomineralization) provide valuable bioinspired templates for the development of advanced biocompatible materials via environmentally benign synthetic routes. Calcium carbonate ($CaCO_3$), the principal inorganic constituent of invertebrate hard tissues, represents a particularly relevant model system for the design of novel biocomposites with potential technological and biomedical applications, including drug delivery. In natural biominerals, calcitic skeletal elements incorporate small amounts of acidic macromolecules, which are known to exert a pronounced influence on $CaCO_3$ polymorphism, morphology, and crystal structure when mineralization is mimicked in vitro, indicating strong and specific interactions at mineral−solution interfaces. In this study, we investigate the role of several classes of low-molecular-weight organic compounds of increasing chemical and structural complexity in the kinetics of calcium carbonate precipitation, with the aim of elucidating the extent and mechanisms of their interfacial interactions. Crystal growth kinetics of well-defined calcite seed crystals were examined in the presence of (i) selected amino acids differing in charge and polarity (aspartic acid, asparagine, lysine, phenylalanine, serine, and alanine), (ii) dipeptides (alanyl-aspartic acid, seryl-aspartic acid, seryl-serine, aspartyl-aspartic acid, and glutamyl-glutamic acid), and (iii) tripeptide aspartic acid derivatives of salicylic acid employed here as a model drug molecule. Analysis of the kinetic data using appropriate crystal growth models enabled the determination and comparison of Langmuir adsorption constants, which were used as quantitative indicators of organic−inorganic interfacial interactions. The results demonstrate that, in addition to molecular charge, hydrophobicity, conformational adaptability, and molecular flexibility play key roles in modulating calcite growth. These findings highlight critical design parameters for the development of efficient and biocompatible drug-derived additives and organic/inorganic composites. Moreover, the applied kinetic approach provides a robust framework for the rational design of biomimetic composite materials.

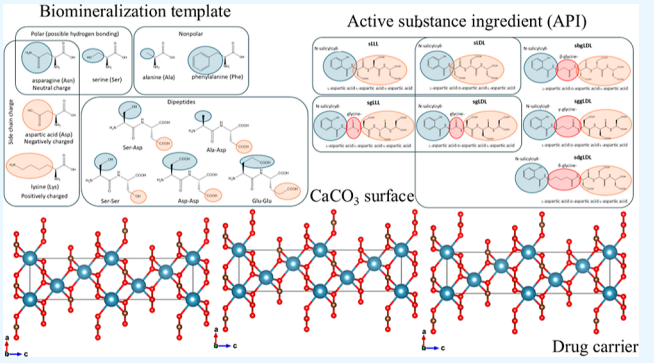

1. INTRODUCTION

A need for novel and advanced materials, as well as for their environmentally friendly synthesis, is constantly growing. Biominerals and processes of their formation in organisms (biomineralization) are a good model for biomimetic-based design and production of new classes of materials.[1−3] One of the most common biominerals, calcium carbonate, precipitates either in a form of unstable hydrated modifications: calcium carbonate hexahydrate ($CaCO_3{\cdot}6H_2O$), calcium carbonate monohydrate ($CaCO_3{\cdot}H_2O$), and amorphous calcium carbonate ($CaCO_3{\cdot}nH_2O$), or as a polymorph: thermodynamically most stable calcite, aragonite, or vaterite. Calcium carbonate phases, particularly vaterite, serve as important in vitro models for biomineralization processes and provide a conceptual and practical link to the design of biocompatible inorganic carriers for drug delivery.[4−12]

In organisms which produce hard tissues, several strategies for controlling the mineralization process have been proposed, involving chemical, spatial, structural, morphological, and/or constructional control.[13] The chemical control assumes the regulation of the ionic composition of the mineralizing compound, as well as the presence of specific macromolecules which may influence the solubility or supersaturation and, consequently, the mechanism of precipitation of the respective mineral. Thus, the researchers give a tremendous effort to study the precipitation of calcium carbonates in the presence of

Received: December 12, 2025
Revised: February 2, 2026
Accepted: February 10, 2026
Published: February 19, 2026

Table 1. Selected Amino Acids and Typical Side Chain Properties[a]

Amino acid	Structural formula	Polarity*	Net charge (pH = 7.9 to 7.2)	Side chain hydrophobicity kcal / mol[36,37]
Serine (Ser)	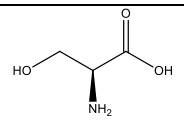	Polar	-0.09 to -0.02	- 0.04
Asparagine (Asn)	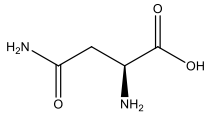	Polar	-0.23 to -0.06	- 0.60
Alanine (Ala)	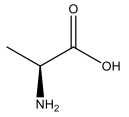	Nonpolar	-0.03 to -0.01	+ 0.31
Phenylalanine (Phe)	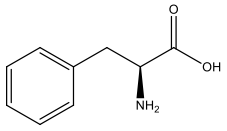	Nonpolar	-0.15 to -0.04	+ 1.79
Aspartic acid (Asp)	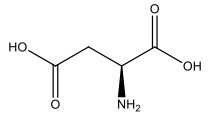	Negatively charged	-1.02 to -1.00	- 0.77
Lysine (Lys)	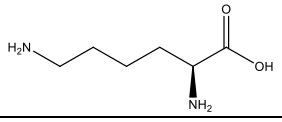	Positively charged	+0.97 to +0.99	- 0.99

[a]Hydrogen bonding refers to the side chain.

different classes of dissolved additives, like synthetic polymers,[14,15] gels,[16,17] or proteins.[18,19] Indeed, the amino acid analyses of the proteins extracted from the nacreous, aragonitic layer of biomineralizing species, like oysters (*Pinctada maxima*, *Pinctada fucata*) or abalones (*Haliotis tuberculata*, *Haliotis rufescens*, *Haliotis laevigata*), indicated their polyanionic (acidic) nature, which enables a strong affinity to bind calcium ions.[20,21] In these proteins, the regions containing not only the acidic amino acids (Asp and Glu) but also the hydrogen-bonding amino acids (Thr, Ser, Tyr, Gln, Asn, and Arg) were identified. Similarly, some in vitro experiments showed that the synthetic analogues of glycoproteins, like poly(aspartic acid) (pAsp) or poly(glutamic acid) (pGlu), also strongly interact with $CaCO_3$ crystal surfaces and cause the changes of precipitation mechanisms and morphologies.[22,23] The chirality of amino acids, like alanine, glycine, proline, valine, or α-aminobutyric acid, has also been found to influence the interfacial interactions with the calcite plane.[47] In addition, the length of polypeptides was found to affect the crystal growth and may cause the stereochemical switch in morphology.[24] Besides the large biomolecules, the influence of small organic compounds like amino acids, which are supposed to be the simplest models of soluble organic matrix molecules, on $CaCO_3$ precipitation has been investigated too.[24−29] The majority of investigations of calcium carbonate interactions with amino acids and their more complex derivatives, inspired by biomineralization, have been performed in spontaneously precipitating systems in which the distinction between nucleation, crystal growth, and aging processes is difficult.[30−35]

In this work, a crystal growth kinetic analysis and seeding experimental setup have been applied in order to investigate the impact of several classes of small molecules with increasing chemical and structural complexity on calcium carbonate precipitation. We assumed that the charge, polarity, conformation, and flexibility of molecules could influence their interactions with growing surfaces. Specifically, the crystal growth kinetics of well-defined calcite seed crystals in the presence of (i) selected amino acids (aspartic acid, asparagine, lysine, phenylalanine, serine, or alanine), (ii) dipeptides (alanyl-aspartic acid, seryl-aspartic acid, seryl-serine, aspartyl-aspartic acid, or glutamyl-glutamic acid), or (iii) salicylic acid adducts with oligopeptides containing aspartic acid and glycine have been investigated. By analysis of the kinetic data and applying the respective growth models, the Langmuir adsorption constants have been calculated, compared, and used as an indication of the extent of organic/inorganic interfacial interactions.

The proposed experimental approach, which comprises the precipitation kinetics analysis, complemented with respective chemical, structural, and morphological analyses, could be recommended as a promising starting point for rational design of new biocompatible organic/inorganic composites, while the peptide adducts of the salicylic could be proposed as a biocompatible model of drug delivery systems.

2. EXPERIMENTAL SECTION

2.1. Materials

The chemicals, $CaCl_2$ and $NaHCO_3$ (both Sigma-Aldrich), used to prepare reactant solutions were analytically pure, and the deionized

https://doi.org/10.1021/acsomega.5c13043
ACS Omega 2026, 11, 14002−14016

Table 2. Selected Dipeptides and Typical Side Chain Properties

Dipeptides	Structural formula	Overall charge (pH = 7.9 to 7.2)	Side chains hydrophobicity* kcal / mol[36,37]
L-aspartyl L-aspartic acid Asp-Asp	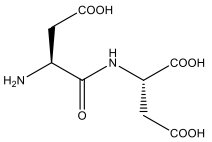	-2.02 - -2.0	-1.54
L-seryl-L-aspartic acid Ser-Asp	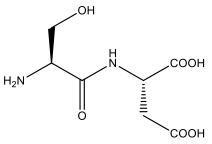	-1.02 - -1.0	-0.81
L-alanyl-L-aspartic acid Ala-Asp	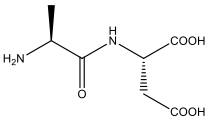	-1.02 - -1.0	-0.46
L-seryl-L-serine Ser-Ser	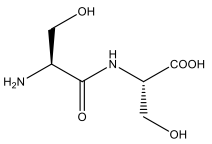	-0.02 – 0.00	-0.08
L-glutamyl-L-glutamic acid Glu-Glu	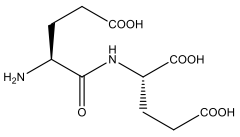	-2.02 - -2.0	-1.28

water was of high quality (conductivity <0.055 μS cm^{-1}). L-Alanine (Sigma), L-serine (Alfa Aesar), L-phenylalanine (Alfa Aesar), L-tyrosine (Alfa Aesar), L-aspartic acid (Alfa Aesar), L-asparagine (Sigma), and L-lysine (Sigma-Aldrich) were used and classified on the basis of their polarity and charge (AA) (Table 1). Dipeptides (L-alanyl-L-aspartic acid (Ala−Asp), L-seryl-L-aspartic acid (Ser−Asp), L-seryl-L-serine (Ser−Ser), L-aspartyl-L-aspartic acid (Asp−Asp), and L-glutamyl-L-glutamic acid (Glu−Glu)) were specifically synthesized and purchased from Bachem (Table 2). The salicylic acid derivatives (*N*-salicyloyl-L-aspartic acid−L-aspartic acid−L-aspartic acid (sLLL), *N*-salicyloyl-L-aspartic acid−D-aspartic acid−L-aspartic acid (sLDL), *N*-salicyloylglycine−L-aspartic acid−L-aspartic acid−L-aspartic acid (sgLLL), *N*-salicyloylglycine−L-aspartic acid−D-aspartic acid−L-aspartic acid (sgLDL), *N*-salicyloyl-*β*-glycine−L-aspartic acid−D-aspartic acid−L-aspartic acid (s*β*gLDL), *N*-salicyloyl-*γ*-glycine−L-aspartic acid−D-aspartic acid−L-aspartic acid (s*γ*gLDL), and *N*-salicyloyl-*δ*-glycine−L-aspartic acid−D-aspartic acid−L-aspartic acid (s*δ*gLDL)) were synthesized according to protocols described in section 2.2 (Table 3).

2.2. Peptide Synthesis

Tripeptides sLLL (*N*-salicyloyl-L-aspartic acid−L-aspartic acid−L-aspartic acid) and sgLLL (*N*-salicyloylglycine−L-aspartic acid−L-aspartic acid−L-aspartic acid) were synthesized by peptide synthesis in solution.

Tripeptides sLDL (*N*-salicyloyl-L-aspartic acid−D-aspartic acid−L-aspartic acid), sgLDL (*N*-salicyloylglycine−L-aspartic acid−D-aspartic acid−L-aspartic acid), s*β*gLDL (*N*-salicyloyl-*β*-glycine−L-aspartic acid−D-aspartic acid−L-aspartic acid), s*γ*gLDL (*N*-salicyloyl-*γ*-glycine−L-aspartic acid−D-aspartic acid−L-aspartic acid), and s*δ*gLDL (*N*-salicyloyl-*δ*-glycine−L-aspartic acid−D-aspartic acid−L-aspartic acid) were synthesized by solid-phase peptide synthesis. The characterization of prepared peptides is shown in the Supporting Information.

2.2.1. Synthesis in Solution. Boc-Asp(OMe)−OH (1.0 mmol) and *N*-hydroxysuccinimide (1.1 mmol) were dissolved in dimethylformamide (DMF) and placed in an ice bath. *N*,*N*′-Dicyclohexylcarbodiimide (1.2 mmol) was dissolved in DMF and added dropwise into the initial solution. The reaction mixture was stirred for 30 min at 0 °C and then at room temperature overnight. The solution was filtered, and the mother liquor was added dropwise into the suspension of H-Asp(OMe)−OH (1.1 mmol) and $KHCO_3$ (1.1 mmol) in water and stirred at room temperature for 2 h. The reaction mixture was filtered, and the filtrate was acidified with citric acid to pH = 2.0. The product was extracted with ethyl acetate, washed with saturated NaCl solution and water, and purified by column chromatography (eluent: ethyl acetate−petrol−acetic acid 5:5:0.5) to give Boc-Asp(OMe)-Asp(OMe)−OH. The isolated dipeptide was resubmitted to the procedure described above with H-Asp(OMe)−OMe to give tripeptide Boc-Asp(OMe)-Asp(OMe)-Asp(OMe)−OMe. Boc deprotection was achieved by treating the tripeptide with TFA/H_2O 9:1. The resulting product was dissolved in methanol and triturated with diisopropyl ether to yield TFAxH-Asp(OMe)-Asp-(OMe)-Asp(OMe)−OMe in 11% overall yield.

2.2.1.1. sLLL. Salicylic acid (0.1 mmol) and *N*-hydroxysuccinimide (0.11 mmol) were dissolved in dimethylformamide (DMF) and placed in an ice bath. *N*,*N*′-Dicyclohexylcarbodiimide (0.12 mmol)

https://doi.org/10.1021/acsomega.5c13043
ACS Omega 2026, 11, 14002−14016

Table 3. Salicylic Derivatives Selected for Kinetic Measurements

Derivates	Structural formula
N-salicyloyl-L-aspartic acid-L-aspartic acid-L-aspartic acid sLLL	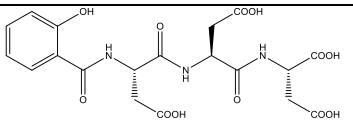
N-salicyloyl-L-aspartic acid-D-aspartic acid-L-aspartic acid sLDL	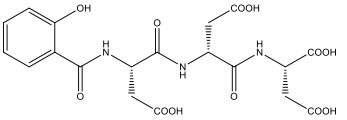
N-salicyloyl-glycine-L-aspartic acid-L-aspartic acid-L-aspartic acid sgLLL	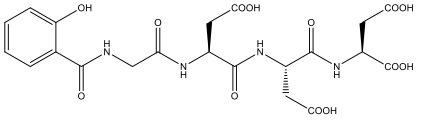
N-salicyloyl-glycine-L-aspartic acid-D-aspartic acid-L-aspartic acid sgLDL	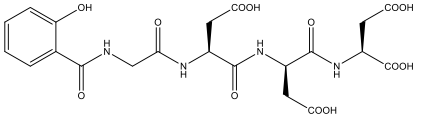
N-salicyloyl-β-glycine-L-aspartic acid-D-aspartic acid-L-aspartic acid sβgLDL	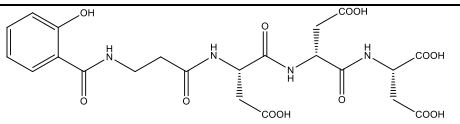
N-salicyloyl-γ-glycine-L-aspartic acid-D-aspartic acid-L-aspartic acid sγgLDL	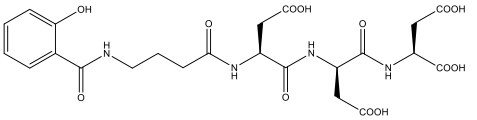
N-salicyloyl-δ-glycine-L-aspartic acid-D-aspartic acid-L-aspartic acid sδgLDL	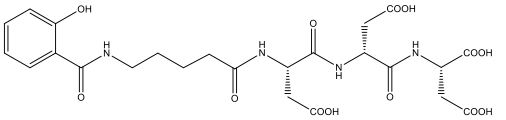

was dissolved in DMF and added dropwise into the initial solution. The reaction mixture was stirred for 30 min at 0 °C and then at room temperature overnight. The solution was filtered, and the mother liquor was added dropwise into the suspension of TFAxH-Asp(OMe)-Asp(OMe)-Asp(OMe)−OMe (0.05 mmol) and $KHCO_3$ (1.1 mmol) in water and stirred at room temperature for 2 h. The reaction mixture was filtered, and the filtrate was acidified with citric acid to pH = 2.0. The product was extracted with ethyl acetate, washed with saturated NaCl solution and water, and purified by column chromatography (eluent: ethyl acetate−petrol−acetic acid 10:5:0.5) to yield Sal-Asp(OMe)-Asp(OMe)-Asp(OMe)−OMe. Ester deprotection was performed with 1.0 M NaOH. After an acid extraction, the product was desalted using a C18 matrix to give pure product (Sal)−L-Asp−L-Asp−L-Asp in 56% yield.

2.2.1.2. sgLLL. Boc-Gly-OH (0.1 mmol) and *N*-hydroxysuccinimide (0.11 mmol) were dissolved in dimethylformamide (DMF) and placed in an ice bath. *N*,*N*′-Dicyclohexylcarbodiimide (0.12 mmol) was dissolved in DMF and added dropwise into the initial solution. The reaction mixture was stirred for 30 min at 0 °C and then at room temperature overnight. The solution was filtered, and the mother liquor was added dropwise into the suspension of TFAxH-Asp(OMe)-Asp(OMe)-Asp(OMe)−OMe (0.05 mmol) and $KHCO_3$ (1.1 mmol) in water and stirred at room temperature for 2 h. The reaction mixture was filtered, and the filtrate was acidified with citric acid to pH = 2.0. The product was extracted with ethyl acetate, washed with saturated NaCl solution and water, and purified by column chromatography (eluent: ethyl acetate−petrol−acetic acid 10:5:0.5) to give Boc-Gly-Asp(OMe)-Asp(OMe)-Asp(OMe)−OMe. Boc deprotection was achieved by treating the tripeptide with TFA/H_2O 9:1. The resulting product was dissolved in methanol and triturated with diisopropyl ether and submitted to the procedure utilizing salicylic acid (2.0 equiv) as described for sLLL to yield (Sal)−Gly−L-Asp−D-Asp−L-Asp in 21% yield (from TFAxH-Asp-(OMe)-Asp(OMe)-Asp(OMe)−OMe).

2.2.2. Solid-Phase Synthesis. Compounds sLDL, sgLDL, sβgLDL, sγgLDL, and sδgLDL were synthesized automatically on a solid-phase peptide synthesizer (Protein Technologies Inc., Tuscon, Arizona, USA) from the C- to N-terminal by the Fmoc method on a commercially available Wang resin (p-alkoxy benzyl alcohol resin, 200−400 mesh, 0.6−1.0 mmol/g resin, Fluka, Buchs, Switzerland) on a 0.1 mmol scale by using the analytical grade amino acids (L-Asp, D-Asp, Gly, *β*-Ala, *γ*-amino butanoic acid, *δ*-amino pentanoic acid) and salicylic acid. The consecutive steps in the solid-phase peptide synthesis performed in each cycle were as follows: (i) deprotection of the Fmoc group by two treatments with 20% piperidine in dimethylformamide (v/v); (ii) coupling by applying HBTU/HOBt/NMM activation and a 3-fold excess of the appropriate Fmoc-amino acid for 1 h; and (iii) removal of the peptides from the resin by treatment with a mixture of TFA−TIS−H_2O in the ratio 9.5:0.25:0.25 (v/v) for 3 h. Successive deprotection and coupling steps were monitored by positive and negative Kaiser (ninhydrin) tests, respectively. The peptide was obtained as a filtrate in trifluoroacetic acid (TFA) and precipitated with cold dry diisopropyl ether. Analysis and purification of crude peptides was achieved by reversed-phase high-performance liquid chromatography (RP HPLC) performed on a Varian 940 LC (Varian Australia Pty Ltd., Mulgrave, Australia)

https://doi.org/10.1021/acsomega.5c13043
ACS Omega 2026, 11, 14002−14016

system using a Eurospher 100 reversed-phase C-18 preparative (250 × 21.2 mM ID, 5 μM, Luna Phenomenex, Torrance, California) (flow rate: 7.0 mL/min) or analytical (250 × 4.5 mM ID, 5 μM, Luna Phenomenex, Torrance, California, USA) (flow rate: 0.5 mL/min) column under isocratic conditions using 10% MeOH in 0.1% aqueous TFA (for solvent systems). UV detection was performed at 215 nm using a Varian 940 LC PDA dual array detector. The TFA ion present after preparative HPLC was removed using a SPE cartridge. The cartridge was first eluted with water and then with MeOH to recover peptide compounds. The eluent was evaporated, and the residue was dissolved in water and lyophilized. Peptides were at least 95% pure as assessed by analytical RP HPLC. Molecular structure was confirmed by mass spectrometry and NMR spectroscopy. NMR spectra were recorded on a Bruker AV 600 spectrometer operating at 150.91 MHz for ^{13}C and 600.13 MHz for S4 for ^{1}H nuclei. The spectra were measured in DMSO-d_6 solutions at 25 °C. Chemical shifts in parts per million were referenced to TMS.

2.3. Precipitation Experiments

Calcium chloride solution was prepared by diluting the appropriate amount of $CaCl_2$ stock solution, while sodium hydrogen carbonate solution was prepared by weighing the appropriate amount of $NaHCO_3$ solid salt. The appropriate amounts of amino acids were dissolved in $NaHCO_3$ solution, while sodium hydroxide (NaOH) or hydrochloric acid (HCl) was used to adjust the pH = 7.9.

The experiments were performed in a thermostated double-walled glass vessel with a 400 cm^3 capacity for amino acids and 20 cm^3 when dipeptides and salicylic acid derivatives have been used. The vessel was tightly closed by a Teflon cover, thus minimizing the exchange of carbon dioxide between the air and the reaction system. The reaction mixture was prepared by mixing equal volumes (200 or 10 cm^3) of $CaCl_2$ and $NaHCO_3$ solutions ($c_i(Ca)_{tot} = c_i(CO_3)_{tot}$ = 5 mmol dm^{-3}; pH_i = 7,9; ϑ = 25 °C). The $CaCl_2$ solution was rapidly added into the $NaHCO_3$ solution containing different AA concentrations. After mixing, the concentrations of both constituting ionic species, calcium and carbonate, were 5 mmol dm^{-3}. The initial concentrations of AAs varied in the range $1 \le c(AA)/\text{mmol dm}^{-3} \le 75$ mmol dm^{-3}, while the initial concentrations of dipeptides varied in the range $10 < c(\text{dipeptide})/\mu\text{mol dm}^{-3} < 1000$ and salicylic derivatives $0{,}5 < c(\text{Salder})/\mu\text{mol dm}^{-3} < 15{,}0$.

The growth of crystals was initiated by inoculation of the metastable solution by the respective amount of well-defined crystal seed. Powder X-ray diffraction analysis of seed material shows that it is pure calcite (Figure S1), with a specific surface area of 2.2 $m^2\ g^{-1}$, as determined by the multiple BET method (Micrometrics, Gemini). The seed material was prepared by a previously proposed method.[26] The amount of added crystal seed has been adjusted in order to provide identical surface area available for growth in each kinetic experiment (0.55 $m^2\ dm^{-3}$). The seed was previously suspended in 500 μL of solution saturated with respect to calcite. The model systems containing the same initial reactant concentrations but without additives were used as controls.

During the experiments, the systems were continuously stirred at a constant rate by means of a magnetic stirrer and thermostated at 25 °C. The progress of the reaction was followed by measuring the pH of the solution using a combined glass−calomel electrode (Radiometer, Red Rod) connected to a digital pH meter (PHM 290, Radiometer). At the end of each experiment, the total volume of suspension was filtered through a 0.22 μM membrane filter (Millipore, cellulose nitrate membrane filters), washed with small portions of water, and dried at 105 °C. The obtained precipitates have been used for structural analysis using FT-IR spectroscopy.[35,38] The concentration of Ca ions in filtrate has been determined by ion chromatography.

Calculations of the ionic composition of the solution at any moment of the crystal growth process were based on continuous pH measurements, relevant charge and mass balance equations for total dissolved calcium (c_{tot}) and carbonate species, as well as the appropriate equilibrium constants.[26] The amount of precipitated calcium carbonate, c_{ppt}, was determined by subtracting the calculated total concentration, c_{tot}, of calcium (or carbonate) species in the closed system from the known initial $CaCl_2$ (or $NaHCO_3$) concentration.

The kinetic data were analyzed by testing the appropriate growth rate mechanisms: (a) spiral growth ($R = k_s(S-1)\ln S$) or (b) surface nucleation ($R = k_e S^{7/6}(S-1)^{2/3}(\ln S)^{1/6}\exp[-K_e/\ln S] \equiv k_e F(S)\exp[-K_e/\ln S]$). The supersaturation was expressed as relative supersaturation, $S-1$, while the saturation ratio, S, was defined as the square root of the quotient of the calcite activity product:

$$S = [(a_{Ca}a_{CO_3})/K_{sp}]^{1/2} \quad (1)$$

in the above expression, a is the activity of the respective ionic species, while K_{sp} is the solubility product of calcite.

The crystal growth rate, R, was calculated by numerical differentiation of the total dissolved calcium concentration, c_{tot}, as a function of time, t, normalized with respect to the surface area of the precipitate, A:

$$R = \frac{1}{A}\frac{dc_{tot}}{dt} \quad (2)$$

The surface area of the precipitate increased during the growth on seed crystals and was calculated by the following expression:

$$A = A_i\left[1 + \frac{c_{ppt}M}{m_i}\right]^{2/3} \quad (3)$$

where A_i is the surface area of the calcite seed (A_i = 2.2 $m^2\ g^{-1}$), m_i is the initially mass of the calcite seed, M is the molar mass of calcium carbonate, and c_{ppt} is the concentration of precipitated calcium carbonate.

3. RESULTS

The mode and extent of interfacial interactions of selected organic additives with mineral surfaces have been revealed from analyses of crystal growth kinetics of the calcite seed, performed in slightly supersaturated precipitation systems. For that purpose, an appropriate amount of the crystal seed has been used, as well as three classes of biocompatible organic molecules of increasing complexity: (i) amino acids, (ii) dipeptides, and (iii) aspartic acid derivatives of salicylic acid. The selection of additives was supposed to allow the distinction of an impact of critical properties of molecules, like charge, polarity, or flexibility.

3.1. Calcite Crystal Growth in a Model System

The kinetic experiments have been performed in the system in which the initial supersaturation was relatively low (S_i = 3.6), and no spontaneous nucleation (precipitation) has been observed within several hours. The absence of nucleation implicates that the growth on calcite seed crystals was the predominant process which caused the measurable changes of pH.[26] Indeed, in all experimental runs, the initial pH was preadjusted to 7.9, which started to decrease immediately after the addition of seed crystals, as can be seen in Figure 1. The reproducibility of the experiments has been confirmed by several runs and the respective coincidence of progress curves.

The crystal growth mechanisms were tested by comparing the growth rate with respective precipitation models, so the obtained linearity for $R = k_s(S-1)\cdot\ln S$ indicates the growth on the spiral step which emerges from the surface dislocations.[39] The average rate constant calculated from the slopes of the straight lines was $k_{s,0}$ = 2.22 ± 0.02 μmol dm^{-3} m^{-2} s^{-1}. The observed continuous growth at relatively low initial supersaturations is typical for crystals containing spiral dislocation and for the absence of surface nucleation. However,

https://doi.org/10.1021/acsomega.5c13043
ACS Omega 2026, 11, 14002−14016

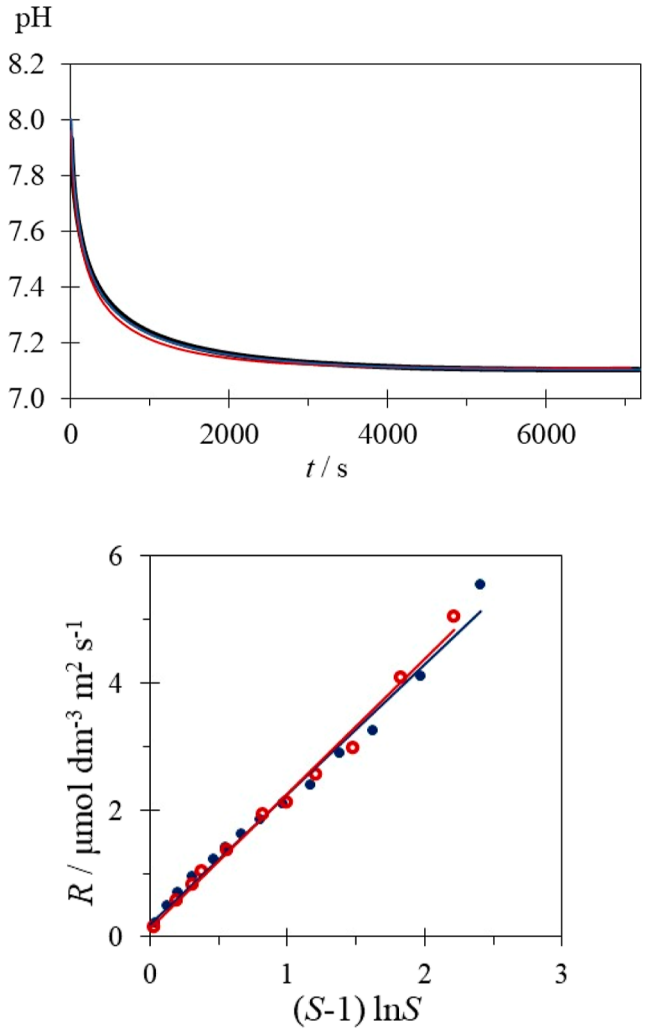

Figure 1. Progress curves, pH vs time, of crystal growth on the calcite seed in the model systems: $c_i(Ca)_{tot} = c_i(CO_3)_{tot}$ = 5 mmol dm^{-3}; pH_i = 7,9; ϑ = 25 °C (top). Test plots for spiral growth mechanisms (growth rate vs function of supersaturation) of respective kinetic runs (down). The amount of seed was 0.55 m^2 dm^{-3}.

the kinetic data are comparable with results shown previously.[26,27]

3.2. Calcite Crystal Growth in the Presence of Amino Acids

The influence of the selected amino acids (Asp, Lys, Asn, Phe, Ser, and Ala) on calcite precipitation has been investigated by their addition into the model system described previously. Figure 2 shows typical progress curves, pH versus time, in the systems containing different concentrations of amino acids. It is evident that, similarly to the model system, calcite started to grow immediately after the seed addition into the reactant solution. Indeed, the precipitation rates in the systems containing the increasing concentrations of amino acids have been progressively reduced (evident as lowering of the slopes), while after a certain period, the growth apparently terminates (the so-called dead zone of growth). The strongest effect could be observed in Asp systems, in which concentrations of AA as low as c = 1.0 mmol dm^{-3} caused significant inhibition of the process, while at the concentration c = 25.0 mmol dm^{-3}, the process was completely inhibited, which is evidenced as no pH change within 6000 s. Electron micrographs of calcite seed crystals isolated from systems containing the corresponding amino acid concentrations, collected after completion of the precipitation process, show no significant morphological changes compared to the reference system nor the formation of new crystals. Furthermore, PXRD analysis indicates that no new polymorphic phases of calcium carbonate were formed, suggesting that crystal growth was the predominant process (Figures S2 and S3).

From the measured pH values, known initial concentrations of reactants, and amount of seed introduced into supersaturated solution, the concentrations and activities of relevant ionic species in solution and the crystal growth rates have been calculated. Figure S4 shows the growth rates plotted as a function of relative supersaturation in the systems containing the selected amino acids. The model systems (bold lines) are shown as well. The values of critical supersaturations (S^*), defined as values when R = 0 for systems with different concentrations of additives, have been estimated from the plots.[40] The obtained linearity of the test plots, in which rate is expressed as a function of reduced supersaturation, S^* (eq 4), showed that in all AA-containing systems, the growth mechanism is identical to that of the model system (surface reaction proceeding at the spiral step). The expression which describes the growth at reduced supersaturation is given by[40]

$$R = k_s(S - 1)(\ln S - \ln S^*) \quad (4)$$

Figure S5 shows the test plots for selected concentrations of Asp-containing systems: the values of the rate constants and critical supersaturations for Asp, but also for all other AAs, are summarized in Table 4. It is evident that the rate constants decrease, while S^* increases with increasing initial AA concentration.

The extent of interfacial interactions of selected amino acids with the calcite seed was tested by applying the model proposed by Kubota and Mullin.[41] The model assumes that the decrease of crystal growth rate at specific solution supersaturation, expressed as R/R_0, is a consequence of two parameters: the relative coverage of active sites at crystal surfaces, θ_{eq}, and the effectiveness factor, α, which is a stereochemical contribution of specific AA molecules to overall growth inhibition. The model is derived from the Langmuir adsorption isotherm and is described by the following equation:

$$R/R_0 = 1 - \alpha[K_{ad}c/(1 + K_{ad}c)] \quad (5)$$

In the above expression, c is the additive concentration, K_{ad} is the Langmuir constant, R is the growth rate at specific supersaturation in the additive-containing system, and R_0 is the growth rate in the model system with no additives, obtained at identical supersaturation.

Figure 3 shows the plots of a representative set of experiments in which relative growth rate reduction of calcite seed crystals is expressed as a function of selected AA concentrations and different supersaturations. The lines drawn through the experimental points are obtained by nonlinearly fitting the data with the function given by eq 5.[41] Both K_{ad} and α are allowed to vary, while the adsorption constant used for each AA was identical for all supersaturations. The obtained values of adsorption parameters, calculated by analysis of the applied growth model, are shown in Table 5. It could be seen that the values of effectiveness factors for all investigated amino acids were higher than 1, which indicates that separation between molecules of adsorbed impurities is approximately of the size of the critical diameter of the surface nucleus on the

https://doi.org/10.1021/acsomega.5c13043
ACS Omega 2026, 11, 14002−14016

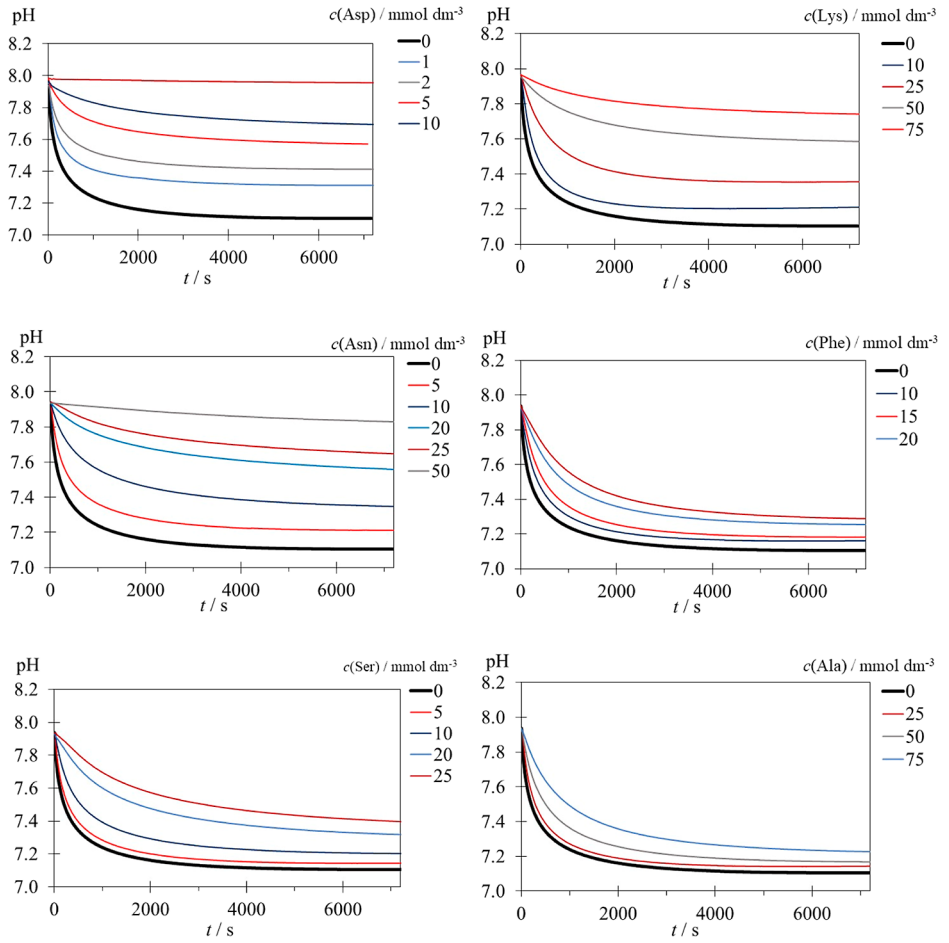

Figure 2. Progress curves, pH vs time, of the crystal growth of the calcite seed in the presence of Asp, Lys, Asn, Phe, Ser, and Ala. The applied concentrations of amino acids, expressed in mmol dm^{-3}, are indicated. Precipitation system: $c_i(Ca)_{tot} = c_i(CO_3)_{tot} = 5$ mmol dm^{-3}, $pH_i = 7{,}9$; $\vartheta = 25$ °C.

growing crystal plane.[41] A significantly higher value of the adsorption constant was obtained for aspartic acid, and it decreased in the order Asp ≫ Asn > Lys > Ser > Phe > Ala, which is consistent with data found previously.[23,31−33]

3.3. Calcite Crystal Growth in the Presence of Dipeptides

In order to test the influence of more complex biomolecules on the calcite crystal growth kinetics, dipeptides (alanyl−aspartic acid, seryl−aspartic acid, seryl−serine, aspartyl−aspartic acid, and glutamyl−glutamic acid) have been used. The respective progress curves, pH vs time, are shown in Figure S6.

The kinetic data were analyzed in analogy to AA systems, and the respective rate constants, as well as the critical supersaturation, were obtained and are shown in Table 6 and Figure S7. Similarly, the experimental data were used to calculate the Langmuir's constants for dipeptides. The results of relative growth rate reduction of the calcite seed determined in the presence of selected dipeptides and at different supersaturations are shown in Figure S8 and Table 7.

The strongest effect, expressed as the highest value of K_{ad}, is observed in the Asp−Asp system, in which dipeptide molecules are double negatively charged (Table 2). However, the K_{ad} value in the Glu−Glu-containing system, which is also double negatively charged, is significantly lower, while the Ser−Ser, without the charged side chain, has a notably lower constant value. The K_{ad} values for dipeptides Ala−Asp and Ser−Asp, which are single negatively charged, are higher than those for Ser−Ser but also notably lower than those for Asp−Asp.

The absence of any consistent correlation between the net charge of molecules and K_{ad} indicates that some other properties of molecules could contribute to their interactions with the surface as well.

3.4. Calcite Crystal Growth in the Presence of Aspartic Acid Derivatives of Salicylic Acid

The tripeptide aspartic acid derivatives of salicylic acid (Salder) were used as an additive in order to try to reveal the roles of chirality and flexibility of molecules relevant in biomineralization and biomineralization-inspired drug design. Therefore, in order to test the chirality of new compounds, two different epimers containing 3 molecules of aspartic acid were synthesized: LDL and LLL. In Table 3, it can be seen that tripeptides (LDL or LLL) and salicylic acid (s) were connected, either directly (sLDL and sLLL) or with a glycine (g) as a linker between them (sgLDL and sgLLL). For investigation of the effect of flexibility, the linker was appropriately extended by the addition of a Gly or CH_2 group: β-glycine (sβgLDL) contains two CH_2 groups, γ-glycine (sγgLDL) three CH_2 groups, and δ-glycine (sδgLDL) four CH_2 groups.

The progress of crystal growth was monitored by monitoring the pH changes from the initial values to values which correspond to near-equilibrium (Figure S9). The obtained rate

https://doi.org/10.1021/acsomega.5c13043
ACS Omega 2026, 11, 14002−14016

Table 4. Rate Constants (k_s) and Critical Supersaturations (S*) Obtained from the Crystal Growth of Calcite in the Presence of Different Concentrations of Selected AAs

amino acid	c(AA)/mmol dm^{-3}	k_s/μmol dm^{-3} m^{-2} s^{-1}	S*
Asp	1.0	2.01	1.69
	2.0	0.98	1.90
	5.0	0.37	2.22
	10.0	0.30	2.50
Lys	10	1.51	1.13
	25	0.98	1.4
	50	1.0	1.78
Asn	5	1.76	1.31
	10	1.36	1.53
	15	1.06	1.68
	20	0.86	1.76
	25	0.75	1.77
Phe	10	1.81	1.16
	25	1.3	1.35
	75	0.91	1.64
Ser	2.5	2.11	1.12
	5.0	2.0	1.21
	10	1.75	1.35
	20	1.22	1.45
Ala	10	2.12	1.08
	25	1.97	1.18
	50	1.67	1.24

constants and critical supersaturation for salicylic acid derivatives are shown in Table 8, while the growth rates expressed as a function of supersaturation are shown in Figure S10. The calculated Langmuir's constants of salicylic acid derivatives and its effectiveness factors are shown in Table 9, while the growth rate reduction at selected supersaturations is shown in Figure S11. The values of obtained K_{ad} values indicated that stronger effects are observed with LDL chirality, while the extension of the linker (sLDL, sgLDL, sβgLDL, sγgLDL, and sδgLDL) does not change them regularly.

4. DISCUSSION

4.1. Inhibition of Calcite Crystal Growth in the Presence of Amino Acids and Dipeptides

We showed previously by applying the spontaneous precipitation experimental setup and using aspartic acid, tyrosine, lysine, asparagine, phenylalanine, serine, and alanine that not only the charged but also the hydrogen bonding (polar) amino acids can strongly interact with the $CaCO_3$ surface, changing the mineralogical composition, structure, and morphology of precipitates.[26]

In this work, we inoculate the calcite crystal seed in order to avoid any unwanted nucleation and formation of new polymorphs in the system, so the obtained effect of amino acids could be attributed exclusively to crystal growth. Thus, from the obtained kinetic data, the spiral growth is confirmed as a controlling mechanism in the model system, and Kubota–Mullin's model has been applied for the calculation of Langmuir adsorption constants. The obtained rate constant ($k_{s,0}$ = 2.22 ± 0.02 μmol dm^{-3} m^{-2} s^{-1}) is consistent with results shown previously in a study by Ukrainczyk et al. in which the authors calculated k_s to be 2.20 ± 0.03 μmol dm^{-3} m^{-2} s^{-1}.[26]

The applied experimental protocol allows the determination of the mechanism of amino acid incorporation into a calcium carbonate crystal. At that, the amino acids' side chain showed the significant role in interactions, observed as inhibition of the crystal growth. Accordingly, AA increased the critical supersaturation and decreased the rate constants. Based on these observations, the mechanism of inhibition, which assumes the amino acid adsorption on the calcite surface, was revealed. Specifically, from the obtained effectiveness factors, the distance between adsorbed amino acid molecules adsorbed on growing crystal steps was estimated to be approximately the same as the critical diameter of the two-dimensional nucleus on the growing plane. In such systems, the step can continue to grow between adsorbed amino acids, as it is predicted with

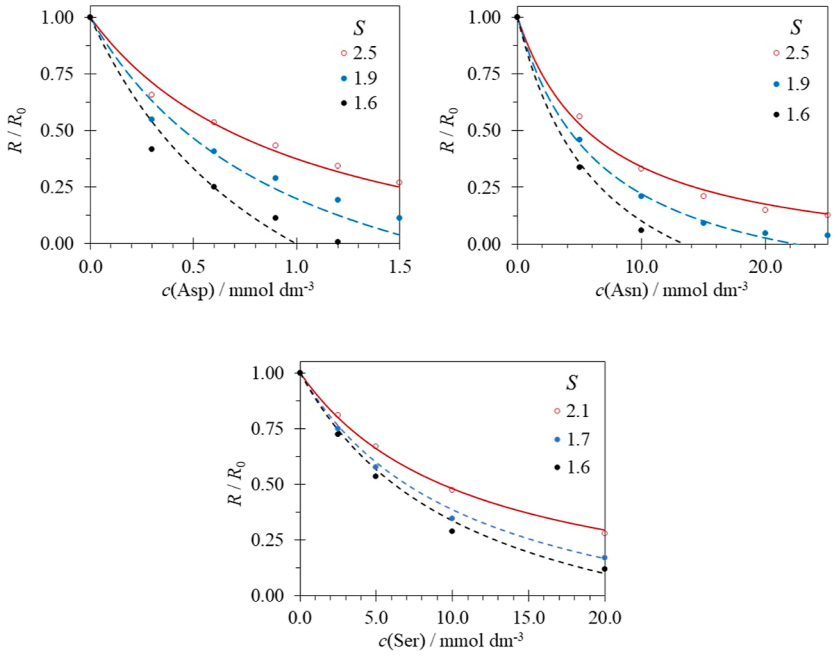

Figure 3. Relative growth rate of calcite seed crystals expressed as a function of selected AA concentrations and different supersaturations, S.

https://doi.org/10.1021/acsomega.5c13043
ACS Omega 2026, 11, 14002−14016

Table 5. Effectiveness Factor (α) and Adsorption Constants (K_{ad}) Obtained from the Crystal Growth of Calcite in the Presence of Different Amino Acids and at Specific Supersaturations

additive	S	α	K_{ad}/dm^3 mmol^{-1}
Asp	2.5	1.25	1.00
	2.3	1.30	
	2.1	1.40	
	1.9	1.60	
	1.7	1.80	
	1.6	2.00	
Lys	2.5	1.05	0.07
	2.3	1.10	
	2.1	1.15	
	1.9	1.20	
	1.7	1.25	
	1.6	1.30	
Asn	2.5	1.10	0.15
	2.3	1.15	
	2.1	1.20	
	1.9	1.30	
	1.7	1.40	
	1.6	1.50	
Phe	2.5	1.15	0.04
	2.3	1.20	
	2.1	1.25	
	1.9	1.30	
	1.7	1.40	
	1.6	1.50	
Ser	2.1	1.10	0.09
	1.9	1.20	
	1.7	1.30	
	1.6	1.40	
Ala	2.5	1.20	0.01
	2.3	1.30	
	2.1	1.40	
	1.9	1.50	
	1.7	1.70	
	1.6	1.80	

Table 6. Kinetic Parameters, Rate Constants (k_s), and Critical Supersaturations (S^*) Obtained from the Crystal Growth of Calcite in the Presence of Different Initial Concentrations of Dipeptides

additive	c(AA) mmol dm^{-3}	k_s/μmol dm^{-3} m^{-2} s^{-1}	S^*
Ala−Asp	0.05	1.95	1.23
	0.1	1.66	1.41
	0.15	1.43	1.53
	0.2	1.25	1.58
	0.25	1.12	1.58
Ser−Asp	0.05	1.77	1.1
	0.1	1.38	1.46
	0.15	1.07	1.76
	0.2	0.84	2
	0.25	0.59	2.18
Ser−Ser	0.1	1.65	1.11
	0.2	1.22	1.26
	0.3	0.92	1.44
	0.4	0.76	1.66
	0.5	0.72	1.91
Asp−Asp	0.01	1.81	1.17
	0.02	1.64	1.32
	0.03	1.49	1.47
	0.04	1.35	1.62
	0.05	1.21	1.76
Glu−Glu	0.02	2	1.22
	0.04	1.8	1.4
	0.06	1.6	1.59
	0.08	1.4	1.78
	0.1	1.21	1.96

Sangwal's model, which describes the crystal growth in solutions containing dissolved additives.[42]

The inhibition effectiveness of the amino acids has also been estimated by correlating the obtained growth rate constants, k_s, with applied concentrations. The values of the rate constants shown as a function of AA concentrations (Table 4 and Figure 4) indicate that in Asp, Asn, Ser, Phe, and Ala systems, k_s linearly decreases with increasing the AA concentration, while in the Lys system, k_s decreases asymptotically. Indeed, the slope of the best lines, $\Delta k_s/\Delta c_{AA}$, could be considered as a growth rate reduction coefficient (GRR) for calcite seed growth, which is, in turn, a measure of inhibition effectiveness of a specific amino acid (μmol dm^{-3} m^{-2} s^{-1}/mmol dm^{-3}). Thus, the GRR values of −0.2416, −0.0643, −0.0535, −0.0393, and −0.0088 have been calculated for Asp, Asn, Ser, Phe, and Ala, respectively.

GRR can be correlated to some typical characteristics of specific AA molecules, like their net charge, z, or side chain hydrophobicity, SCH (Table 1). It could be seen that all AAs are negatively charged at the applied pH of the solution, and the only exception is Lys, which is positively charged at 7.2 < pH < 7.9 (z = +0.96).[a] It should also be emphasized that in the investigated model precipitation system, in which the concentrations of calcium and carbonate ions are identical, c = 5 mmol dm^{-3}, and 7.2 < pH < 7.9, the surface of calcite seed crystals is positively charged, as determined by electrokinetic measurements (15.0 mV < ζ < 14.0 mV).[26]

Growth rate reduction coefficients, GRR, of amino acids plotted as a function of respective net charge, z, are shown in Figure 5. It is evident that the inhibition efficiency of Asp is significantly higher than for other additives, while for Ala, the inhibition efficiency is the lowest. The explanation could be related to the significantly higher value of negative charge of Asp molecules (z = −1.02 at pH = 7.9), which provides the strongest electrostatic attractions with positively charged calcite surfaces. Indeed, literature data suggested that Asp could efficiently disrupt the hydration layer and, consequently, enable stronger interactions with calcite surfaces.[32,43] On the other hand, no correlation between GRR and side chain hydrophobicity could be found (Figure S12).

However, the differences between extents of interactions, seen as a difference in the inhibition of calcite growth, can be attributed to the difference in polarity of amino acid side chains. An increase of the adsorption constant values for selected amino acids was observed in the order Asp > Asn > Ser > Lys > Phe > Ala. The highest K_{ad} value was 1.00 mmol^{-1} dm^3, which was obtained for Asp (Figure S13). This value is in good correlation with the adsorption constant of N-Sal-Asp obtained by Ukrainczyk et al. (K_{ad} = 1.63 mmol^{-1} dm^3).[26] The higher value indicates the strongest interactions between Asp and the surface of calcite, which can be explained as a synergistic interaction of two Asp carbonyl groups.[32] In the case of Asn, the interactions were much weaker but were still

https://doi.org/10.1021/acsomega.5c13043
ACS Omega 2026, 11, 14002−14016

Table 7. Effectiveness Factor (α) and Adsorption Constants (K_{ad}) Obtained from the Crystal Growth of Calcite in the Presence of Different Dipeptides and at Specific Supersaturations

additive	S	α	K_{ad}/dm^3 mmol^{-1}
Ala−Asp	2.5	1.40	6.00
	2.3	1.50	
	2.1	1.60	
	1.9	1.70	
	1.7	1.90	
	1.6	2.10	
Ser−Asp	2.5	1.60	6.10
	2.3	1.70	
	2.1	1.80	
	1.9	1.90	
	1.7	2.00	
	1.6	2.10	
Ser−Ser	2.5	1.40	3.70
	2.3	1.45	
	2.1	1.50	
	1.9	1.55	
	1.7	1.60	
	1.6	1.70	
Asp−Asp	2.5	1.05	50.00
	2.3	1.10	
	2.1	1.15	
	1.9	1.25	
	1.7	1.35	
	1.6	1.45	
Glu−Glu	2.5	1.20	20.00
	2.3	1.25	
	2.1	1.30	
	1.9	1.40	
	1.7	1.60	
	1.6	1.80	

Table 8. Kinetic Parameters, Rate Constants (K_s), and Critical Supersaturations (S^*) Obtained from the Crystal Growth of Calcite in the Presence of Different Initial Concentrations of Salicylic Acid Derivatives

additive	c(AA) mmol dm^{-3}	k_s/μmol dm^{-3} m^{-2} s^{-1}	S^*
sLDL	0.001	1.91	1.41
	0.002	1.76	1.65
	0.003	1.61	1.86
	0.004	1.46	2.02
	0.005	1.31	2.16
sLLL	0.001	2.01	1.36
	0.0025	1.95	1.6
	0.004	1.89	1.89
	0.006	1.83	2.06
	0.008	1.78	2.25
sgLDL	0.001	1.92	1.4
	0.002	1.81	1.61
	0.003	1.71	1.78
	0.004	1.63	1.93
	0.006	1.53	2.15
sgLLL	0.001	1.95	1.35
	0.002	1.85	1.56
	0.003	1.76	1.75
	0.004	1.7	1.91
	0.005	1.65	2.04
sβgLDL	0.001	1.93	1.34
	0.002	1.83	1.56
	0.003	1.74	1.74
	0.004	1.67	1.9
	0.005	1.62	2.04
sγgLDL	0.001	2.01	1.39
	0.002	1.86	1.59
	0.003	1.74	1.76
	0.004	1.65	1.91
	0.005	1.59	2.03
sδgLDL	0.001	1.78	1.36
	0.002	1.68	1.55
	0.003	1.59	1.73
	0.004	1.52	1.87
	0.005	1.40	2.07

higher than for other amino acids, which is a consequence of amide group polarity.[33] If we compare the influence of Asp, Asn, and Lys with the charge of their side chain, it can be seen that Lys has the weakest interaction with calcite. However, interactions of Ser are stronger than those of Lys, probably as a consequence of the polarity of the OH group. Indeed, Phe and Ala, with nonpolar side groups, show weaker interactions with calcite as a consequence of limited hydrogen bonding with the calcite surface. Such interactions are stronger in the case of Asp, Asn, Ser, and Lys, having polar side groups. Based on the given results, it can be concluded that not only can acidic amino acids strongly influence the calcite growth, but also the hydrogen bonding established between the amino acid's side chain and the calcium carbonate surface has a significant role.

In order to investigate whether the interactions between biomolecules and calcite could be increased by increasing their size and complexity, we performed similar precipitation experiments using the dipeptides as additives. The results showed that dipeptides had a stronger effect than amino acids alone, which indicates the synergistic effect. Similar observations were obtained previously in aspartic acid oligopeptides' systems, in which K_{ad} increased by an order of magnitude per added Asp molecule (K_{ad}(Asp) = 1.0 dm^3 mmol^{-1}; K_{ad} (Asp$_2$); = 58.5 dm^3 mmol^{-1}; K_{ad} (Asp$_3$). = 397.2 dm^3 mmol^{-1}).[44] The values of constants for Asp and Asp−Asp obtained in this study and previously are in good correlation. To understand the effect of Ala (nonpolar) and Ser (polar), we tested dipeptides containing Asp. The Ser−Asp has a constant value slightly higher than Ala−Asp, thus emphasizing the importance of an additional OH group in interaction with the calcite surface. A similar effect was shown by spontaneous precipitation experiments.[35] However, Ser−Ser is weakly adsorbed on the calcite surface, thus confirming the importance of the carboxylic group for adsorption. Thus, the effects of dipeptides containing two carboxylic groups (Glu−Glu and Asp−Asp) are stronger than the effects of other dipeptides, thus indicating that a synergistic effect between the side chain and the C-terminus group is also important. Such conclusions are supported with some previous investigation in which adsorption constants of different carboxylic and dicarboxylic acids have been compared.[45] In these systems, the addition of $-CH_2$ groups between carboxylic groups caused the decrease of adsorption. However, some previous research on salicylic acid derivatives with aspartic acid and glutamic acid showed that more efficient binding is observed with Sal−Asp (K_{ad} = 1.6 dm^3 mmol^{-1}) than Sal−Glu (K_{ad} = 0.8 dm^3 mmol^{-1}).[26]

https://doi.org/10.1021/acsomega.5c13043
ACS Omega 2026, 11, 14002−14016

Table 9. Effectiveness Factor (α) and Adsorption Constants (K_{ad}) Obtained from the Crystal Growth of Calcite in the Presence of Different Sal Derivatives and at Specific Supersaturations

additive	S	α	K_{ad}/dm^3 mmol^{-1}
sLDL	2.5	1.05	1000
	2.3	1.10	
	2.1	1.20	
	1.9	1.30	
	1.7	1.40	
sLLL	2.5	1.01	600
	2.3	1.05	
	2.1	1.10	
	1.9	1.20	
	1.7	1.30	
sgLDL	2.5	1.005	850
	2.3	1.01	
	2.1	1.05	
	1.9	1.15	
	1.7	1.25	
sgLLL	2.5	1.05	550
	2.3	1.10	
	2.1	1.20	
	1.9	1.30	
	1.7	1.40	
sβgLDL	2.3	1.05	700
	2.1	1.10	
	1.9	1.20	
	1.7	1.30	
sγgLDL	2.5	1.01	750
	2.3	1.05	
	2.1	1.10	
	1.9	1.20	
	1.7	1.30	
sδgLDL	2.3	1.01	800
	2.1	1.05	
	1.9	1.10	
	1.7	1.20	

Figure S14 shows the growth rate constants of Asp−Asp, Glu−Glu, Asp−Ser, Asp−Ala, and Ser−Ser containing systems, expressed as a function of their initial concentration in solution. It can be seen that for all dipeptide molecules, k_s linearly decreases with increasing concentration, and the highest slope (growth rate reduction coefficients, GRR) has been obtained for negatively charged molecules (Asp−Asp and Glu−Glu), while the lowest GRR has the molecule which is virtually neutral at a given pH (Ser−Ser).[b] More specifically, GRR values of 12.69, 9.41, 6.92, 4.86, and 3.63 have been determined for Asp−Asp, Glu−Glu, Asp−Ser, Asp−Ala, and Ser−Ser, respectively.

When the growth rate reduction coefficients are expressed as a function of the respective net charge of dipeptides (Figure S15), no linear correlation can be observed, but good correlation is obtained when side chain hydrophobicities are considered, as evident in Figure 6. At that, side chain hydrophobicity of a single amino acid is an experimentally measured transfer free energy of each amino acid between octanol and water, subtracted from the value of the transfer free energy of Gly, identical to 0 kcal mol^{-1}.[36,37]

4.2. Inhibition of Calcite Crystal Growth in the Presence of Aspartic Acid Derivatives of Salicylic Acid

We showed previously[26,27] that molecules in which Asp and Glu are linked to salicylic acid influence the crystal growth kinetics of calcite crystals more efficiently than only salicylic acid or its derivatives. From the calculated growth rate and adsorption constants, we concluded that the adsorption of salicylic acid derivatives is much stronger, which indicates that the modification of specific molecules with acidic amino acid motifs could significantly improve their binding at mineral surfaces. By considering these findings and the results of the adsorption constants of amino acids and dipeptides shown above, we prepared the respective salicylic acid adducts with polypeptides containing aspartic acid and glycine. We estimated that such modification of model drug molecules can enhance their uptake by the mineral phase during the mineralization process and likely influence the functionality of desired organic−inorganic composite materials.

At applied experimental conditions, the adduct molecules hold identical net charges and hydrophobicities since they are built up from identical drug molecules, salicylic acid, and aspartic acid tripeptide with four deprotonated carboxylic groups ($z \approx -4$). Molecules also contain different numbers of glycine linkers (1 to 4), which have, by definition, identical hydrophobicity, equal to 0 kcal mol^{-1}. However, the aspartic acid tripeptides have either LDL or LLL conformation, while different numbers of glycine linkers are supposed to contribute to the flexibility of molecules. Figure S16 shows the crystal growth rate constants of sLLL, sLDL, sgLDL, sgLLL, sβgLDL, sγgLDL, and sδgLDL, expressed as a function of their initial concentration in the precipitation systems. Indeed, k_s linearly decreases in all systems, and the slopes of the best lines are considered to be the GRR. The highest value of the GRR has been obtained for sLDL (GRR = −150 μmol dm^{-3} m^{-2} s^{-1}/mmol dm^{-3}), the lowest for sLLL (GRR = −33 μmol dm^{-3} m^{-2} s^{-1}/mmol dm^{-3}), while for the other additives, no significant difference could be observed, and GRR varied within a range from −75 to −78 μmol dm^{-3} m^{-2} s^{-1}/mmol dm^{-3}.

Figure 7 shows the GRR coefficients of adducts, plotted as a function of the number of glycine linkers. It is evident that the strongest inhibition effect has been observed when the molecule without glycine linkers and LDL conformation has been used (sLDL), while the weakest interfacial interactions with calcite surfaces were obtained with sLLL diastereomers. Indeed, in the sLDL molecule, three side-chain carboxylic groups are oriented on the same side, which contributes to higher charge density and, consequently, possible enhanced electrostatic contribution in interfacial interactions. On the other hand, when the glycine linker is introduced, no significant difference in the effects of LDL and LLL diastereomers could be detected. GRR coefficients of Sal derivatives with an increasing number of Gly linkers are practically identical, which indicates that in this specific case, the flexibility of molecules does not consistently contribute to surface interactions. Such findings are apparently in contradiction with the results of the investigation of carboxylic diacid described in literature,[45] which showed that the values of the respective Langmuir constants started to increase after the introduction of more than three CH_2 groups as a consequence of the flexibility of the molecules.

Indeed, some preliminary results of molecular modeling[46] indicated that derivatives with LDL are in the minima of free

https://doi.org/10.1021/acsomega.5c13043
ACS Omega 2026, 11, 14002−14016

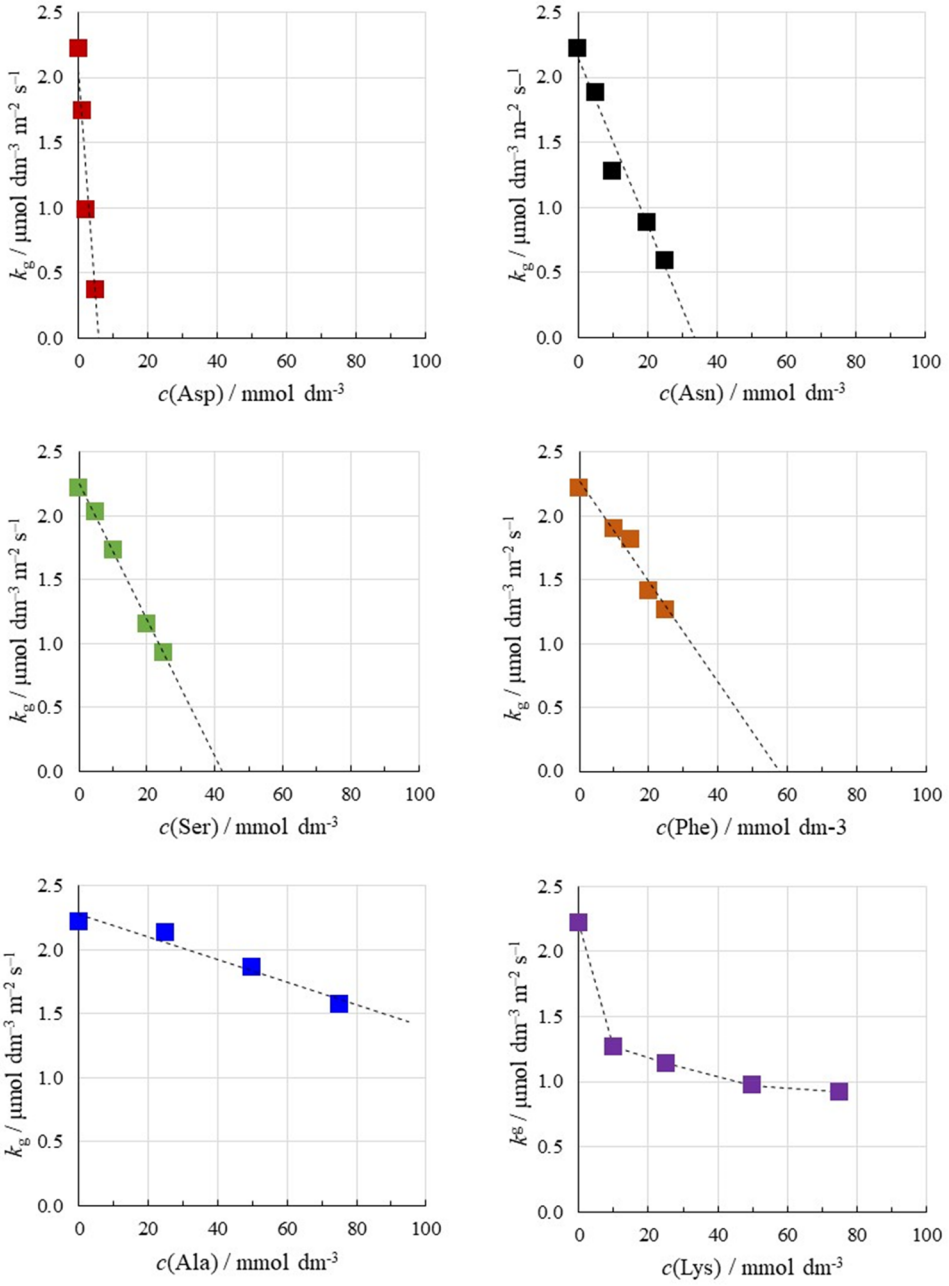

Figure 4. Values of the rate constant, k_g, of calcite crystals obtained for the growth in the presence of different concentrations of amino acids in a precipitation system: $c_i(Ca)_{tot} = c_i(CO_3)_{tot}$ = 5 mmol dm^{-3}, pH_i = 7,9 i ϑ = 25 °C.

energy in a bulk region and bind more strongly on the calcite surface than LLL. The reason for stronger bonding is most probably because of LDL binding on the surface with four carboxylic groups (COOH), while LLL makes a bond only with 3 groups. The influence of chirality on binding to the calcite surface was also investigated by Orme,[47] who found that the stronger bonding energy of D-Asp than L-Asp was obtained on a flat surface. To further understand the binding mechanisms, detailed MD modeling, performed on different calcite surfaces, needs to be done. Namely, we suggested previously that in a case of aspartic acid-containing peptides, the most realistic binding environment is not the flat surfaces but the growing island on the 104 calcite surface.[44]

The results of adsorption constant determination from analysis of crystal growth kinetics showed that the selected salicylic acid derivatives bind much stronger than dipeptides and amino acids. The effect was explained by the presence of additional carboxylic groups in molecules that interact with the calcite surface. The obtained results are consistent with the results of the growth rate reduction determination. Indeed, Figure S13 shows that by increasing the number of carboxylic groups that could interact with surfaces, the values of adsorption constants of three classes of compounds consistently increase: amino acids, dipeptides, and salicylic acid adducts with acidic AA. However, it should be emphasized that the literature data confirm that not only dissolved molecules but also suspended nanoparticles, vesicles, or oil droplets stabilized by multiple carboxyl groups adsorb much more efficiently onto the calcite surface. This enhanced adsorption subsequently leads to significant occlusion within the crystal

https://doi.org/10.1021/acsomega.5c13043
ACS Omega 2026, 11, 14002−14016

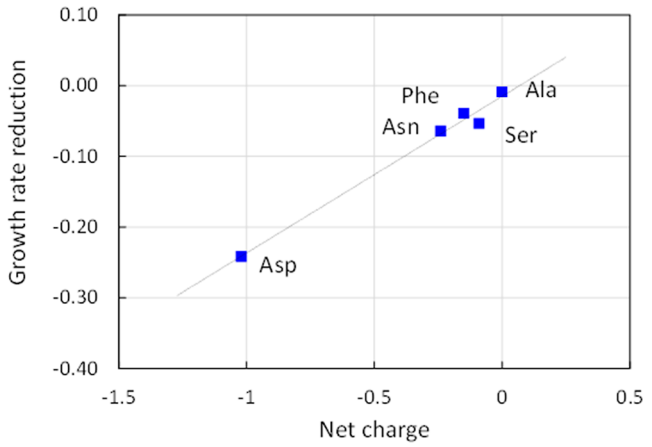

Figure 5. Growth rate reduction coefficients expressed as a function of total net charge of the respective AA molecules.

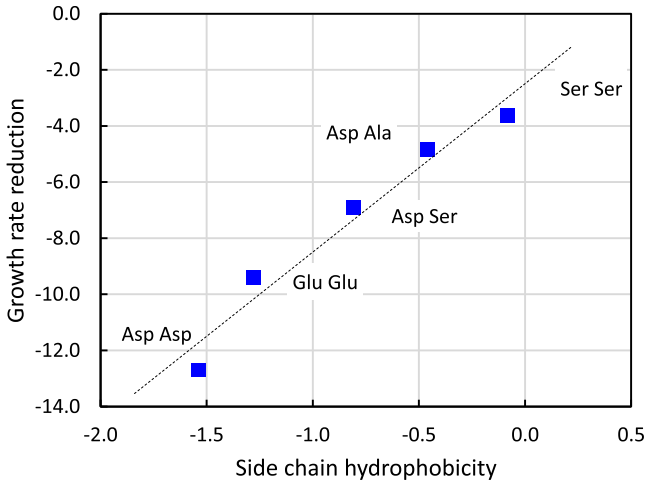

Figure 6. Values of growth rate reduction coefficients expressed as a function of side chain hydrophobicity of the respective dipeptide molecules.

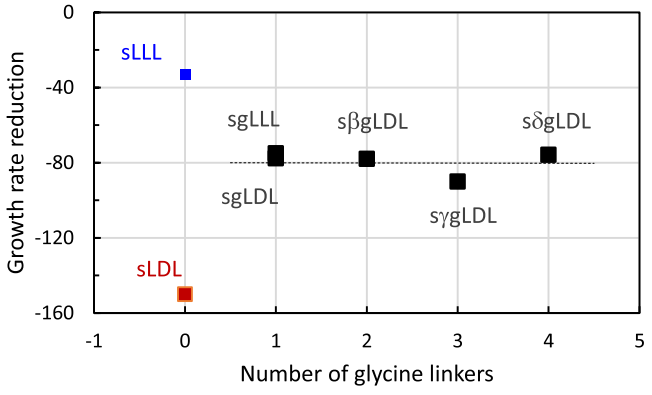

Figure 7. Values of growth rate reduction coefficients expressed as a function of the number of glycine linkers of respective aspartic acid tripeptide derivatives of salicylic acid.

lattice. In particular, vesicles decorated with anionic carboxylate groups are occluded more efficiently within calcite compared to those exhibiting surface phosphate, sulfate, or sulfonate groups.[48−50]

5. CONCLUSIONS

Calcite crystal growth kinetics was investigated in a model system employing as additives three classes of small organic molecules of increasing structural complexity, amino acids, dipeptides, and amino acid-based salicylic acid derivatives. Such an approach enabled a systematic analysis of the mode and extent of organic−inorganic interfacial interactions relevant to biomineralization processes but also to the rational design of functional organic−inorganic composite materials with potential biomedical applications, including drug delivery systems.

Tripeptide derivatives of salicylic acids were synthesized as model drug molecules. Langmuir adsorption constants (K_{ad}) for selected amino acids, dipeptides, and aspartic acid-based tripeptide derivatives of salicylic acid were determined from calcite crystal growth kinetic data.

For the investigated amino acids, the strength of interaction with the calcite surface decreased in the order Asp > Asn > Ser > Lys > Phe > Ala. The interaction intensity was found to correlate with the net charge of the amino acids under the experimental conditions, highlighting the dominant role of electrostatic interactions for small molecules.

Dipeptides (alanyl−aspartic acid, seryl−aspartic acid, seryl−serine, aspartyl−aspartic acid, and glutamyl−glutamic acid) exhibited significantly stronger interactions with calcite surfaces compared to their corresponding amino acids, as evidenced by enhanced crystal growth inhibition and higher Langmuir adsorption constants. Among the studied dipeptides, Asp−Asp showed the strongest inhibitory effect on calcite growth, followed by Glu−Glu, while Ser−Ser exhibited the weakest effect. The interaction strengths of the dipeptides could be correlated to the hydrophobicity of their side chains.

Aspartic acid-based tripeptide derivatives of salicylic acid displayed the strongest interactions with calcite surfaces, with Langmuir adsorption constants several orders of magnitude higher than those obtained for amino acids, dipeptides, or salicylic acid alone. Kinetic data further demonstrated that both the chirality and molecular flexibility of the model drug derivatives can be exploited to tune their adsorption affinity toward mineral surfaces, supporting their potential use in mineral-based drug carrier systems.

Overall, the obtained kinetic (k_s) and adsorption (K_{ad}) parameters, together with the applied crystal growth kinetics approach, provide valuable insight into the molecular interactions between carboxylate-containing model drug derivatives and mineral surfaces. These findings establish a rational framework for the design of functional organic−inorganic composites. While charge and hydrophobicity dominate interfacial interactions for small molecules, larger and more complex molecules exhibit a complex interplay of charge, hydrophobicity, flexibility, and their mutual coupling, leading to increasingly complex and less predictable adsorption behavior at mineral interfaces.

■ ASSOCIATED CONTENT

Supporting Information

The Supporting Information is available free of charge at https://pubs.acs.org/doi/10.1021/acsomega.5c13043.

Characterization of synthesized peptides and crystal seed, crystal growth kinetics, and growth rate reduction (PDF)

https://doi.org/10.1021/acsomega.5c13043
ACS Omega 2026, 11, 14002−14016

AUTHOR INFORMATION

Corresponding Author

Damir Kralj − *Laboratory for Precipitation Processes, Division of Materials Chemistry, Ruđer Bošković Institute (RBI), 10002 Zagreb, Croatia;* orcid.org/0000-0002-4152-4893; Email: kralj@irb.hr

Authors

Lara Jurković − *Laboratory for Precipitation Processes, Division of Materials Chemistry, Ruđer Bošković Institute (RBI), 10002 Zagreb, Croatia;* orcid.org/0000-0001-7229-9054

Andreja Jakas − *Laboratory for Chiral Technologies, Division of Organic Chemistry and Biochemistry, Institut Ruder Boskovic, 10000 Zagreb, Croatia*

Matija Gredičak − *Laboratory for Synthetic Methodologies in Organic Chemistry, Division of Organic Chemistry and Biochemistry, Institut Ruder Boskovic, 10000 Zagreb, Croatia;* orcid.org/0000-0002-6306-5210

Complete contact information is available at: https://pubs.acs.org/10.1021/acsomega.5c13043

Author Contributions

L.J.: data curation; formal analysis; investigation; writing—original draft. A.J.: data curation; formal analysis. M.G.: data curation; formal analysis. D.K.: conceptualization; data curation; formal analysis; investigation; methodology; funding acquisition; project administration; writing—original draft; review and editing; supervision.

Notes

The authors declare no competing financial interest.

ACKNOWLEDGMENTS

The Croatian Science Foundation is gratefully acknowledged for the financial support (D.K.: Project IP-2013-11-5055). We thank Z. Brkljača (RBI) for discussion about molecular modeling of the calcite surfaces.

ABBREVIATIONS

AA, amino acid; Sal, salicylic acid; Sal-der, tripeptide aspartic acid derivatives of salicylic acid; sLLL, *N*-salicyloyl-L-aspartic acid−L-aspartic acid−L-aspartic acid; sLDL, *N*-salicyloyl-L-aspartic acid−D-aspartic acid−L-aspartic acid; sgLLL, *N*-salicyloylglycine−L-aspartic acid−L-aspartic acid−L-aspartic acid; sgLDL, *N*-salicyloylglycine−L-aspartic acid−D-aspartic acid−L-aspartic acid; sbgLDL, *N*-salicyloyl-*β*-glycine−L-aspartic acid−D-aspartic acid−L-aspartic acid; sggLDL, *N*-salicyloyl-*γ*-glycine−L-aspartic acid−D-aspartic acid−L-aspartic acid; sdgLDL, *N*-salicyloyl-*δ*-glycine−L-aspartic acid−D-aspartic acid−L-aspartic acid; GRR, growth rate reduction coefficient

ADDITIONAL NOTES

[a]The net charge is calculated by considering the appropriate dissociation constants of AA ionic species at specific pH. [b]The net charge of dipeptide molecules has been estimated by summation of charges of individual AA molecules.

REFERENCES

(1) Nudelman, F.; Sommerdijk, N. A. J. M. Biomineralization as an Inspiration for Materials Chemistry. *Angew. Chem., Int. Ed.* **2012**, *51* (27), 6582−6596.

(2) Estroff, L. A. Introduction: Biomineralization. *Chem. Rev.* **2008**, *108*, 4329−4331.

(3) Weber, E.; Pokroy, B. Intracrystalline Inclusions within Single Crystalline Hosts: From Biomineralization to Bio-Inspired Crystal Growth. *CrystEngComm* **2015**, *17* (31), 5873−5883.

(4) Declet, A.; Reyes, E.; Suarez, O. M. Calcium Carbonate Precipitation: A Review of the Carbonate Crystallization Process and Applications in Bioinspired Composites. *Rev. Adv. Mater. Sci.* **2016**, *44*, 87−107.

(5) Meldrum, F. C.; Colfen, H. Controlling Mineral Morphologies and Structures in Biological and Synthetic Systems. *Chem. Rev.* **2008**, *108*, 4332−4432.

(6) Côté, A. S.; Darkins, R.; Duffy, D. M. Deformation Twinning and the Role of Amino Acids and Magnesium in Calcite Hardness from Molecular Simulation. *Phys. Chem. Chem. Phys.* **2015**, *17*, 20178−20184.

(7) Liu, Y.; Yuan, W.; Shi, Y.; Chen, X.; Wang, Y.; Chen, H.; Li, H. Functionalizing Single Crystals: Incorporation of Nanoparticles inside Gel-Grown Calcite Crystals. *Angew. Chem., Int. Ed.* **2014**, *53*, 4127−4131.

(8) Milita, S.; Zaquin, T.; Fermani, S.; Montroni, D.; Pinkas, I.; Barba, L.; Falini, G.; Mass, T. Assembly of the Intraskeletal Coral Organic Matrix during Calcium Carbonate Formation. *Cryst. Growth Des.* **2023**, *23*, 5801.

(9) Ueno, Y.; Futagawa, H.; Takagi, Y.; Ueno, A.; Mizushima, Y. Drug-Incorporating Calcium Carbonate Nanoparticles for a New Delivery System. *J. Controlled Release* **2005**, *103* (1), 93−98.

(10) Than, M. M.; Lawanprasert, P.; Jateleela, S. Utilization of Eggshell Powder as Excipient in Fast and Sustained Release Acetaminophen Tablets. *Pharm. Sci. Asia* **2020**, *39* (3−4), 32−38.

(11) Ferreira, A. M.; Vikulina, A. S.; Volodkin, D. CaCO3 Crystals as Versatile Carriers for Controlled Delivery of Antimicrobials. *J. Controlled Release* **2020**, *328* (July), 470−489.

(12) Niu, Y. Q.; Liu, J. H.; Aymonier, C.; Fermani, S.; Kralj, D.; Falini, G.; Zhou, C. H. Calcium Carbonate: Controlled Synthesis, Surface Functionalization, and Nanostructured Materials. *Chem. Soc. Rev.* **2022**, *51* (18), 7883−7943.

(13) Mann, S. *Biomirealization: Principles and Concepts in Bioinorganic Materials Chemistry*; Oxford University Press: New York, 2001.

(14) Kim, Y. Y.; Semsarilar, M.; Carloni, J. D.; Cho, K. R.; Kulak, A. N.; Polishchuk, I.; Hendley, C. T.; Smeets, P. J. M.; Fielding, L. A.; Pokroy, B.; Tang, C. C.; Estroff, L. A.; Baker, S. P.; Armes, S. P.; Meldrum, F. C. Structure and Properties of Nanocomposites Formed by the Occlusion of Block Copolymer Worms and Vesicles Within Calcite Crystals. *Adv. Funct. Mater.* **2016**, *26* (9), 1382−1392.

(15) Kirboga, S.; Öner, M. The Inhibitory Effects of Carboxymethyl Inulin on the Seeded Growth of Calcium Carbonate. *Colloids Surf. B Biointerfaces* **2012**, *91* (1), 18−25.

(16) Manoli, F.; Dalas, E. The Effect of Sodium Alginate on the Crystal Growth of Calcium Carbonate. *J. Mater. Sci. Med.* **2002**, *13* (2), 155−158.

(17) Ritchie, A. W.; Watson, M. I. T.; Turnbull, R.; Lu, Z. Z.; Telfer, M.; Gano, J. E.; Self, K.; Greer, H. F.; Zhou, W. Reversed Crystal Growth of Rhombohedral Calcite in the Presence of Chitosan and Gum Arabic. *CrystEngComm* **2013**, *15* (47), 10266.

(18) Weber, E.; Guth, C.; Weiss, I. M. GFP Facilitates Native Purification of Recombinant Perlucin Derivatives and Delays the Precipitation of Calcium Carbonate. *PLoS One* **2012**, *7* (10), No. e46653.

(19) Weber, E.; Bloch, L.; Guth, C.; Fitch, A. N.; Weiss, I. M.; Pokroy, B. Incorporation of a Recombinant Biomineralization Fusion Proteininto the Crystalline Lattice of Calcite. *Chem. Mater.* **2014**, *26*, 4925−4932.

https://doi.org/10.1021/acsomega.5c13043
ACS Omega 2026, 11, 14002−14016

(20) Michenfelder, M.; Fu, G.; Lawrence, C.; Weaver, J. C.; Wustman, B. A.; Taranto, L.; Evans, J. S.; Morse, D. E. Characterization of Two Molluscan Crystal-Modulating Biomineralization Proteins and Identification of Putative Mineral Binding Domains. *Biopolymers* **2003**, *70* (4), 522−533.
(21) Adamiano, A.; Bonacchi, S.; Calonghi, N.; Fabbri, D.; Falini, G.; Fermani, S.; Genovese, D.; Kralj, D.; Montalti, M.; NjegićDžakula, B.; Prodi, L.; Sartor, G. Structural Changes in a Protein Fragment from Abalone Shell during the Precipitation of Calcium Carbonate. *Chem.—Eur. J.* **2012**, *18* (45), 14367−14374.
(22) Njegic, B.; Brečević, L.; Falini, G.; Kralj, D. Calcite Crystal Growth Kinetics in the Presence of Charged Synthetic Polypeptides. *Cryst. Growth Des.* **2009**, *9*, 2425−2434.
(23) Elhadj, S.; Salter, E. A.; Wierzbicki, A.; De Yoreo, J. J.; Han, N.; Dove, P. M. Peptide Controls on Calcite Mineralization: Polyaspartate Chain Length Affects Growth Kinetics and Acts as a Stereochemical Switch on Morphology. *Cryst. Growth Des.* **2006**, *6* (1), 197−201.
(24) Dalas, E.; Chalias, A.; Gatos, D.; Barlos, K. The Inhibition of Calcium Carbonate Crystal Growth by the Cysteine-Rich Mdm2 Peptide. *J. Colloid Interface Sci.* **2006**, *300* (2), 536−542.
(25) Malkaj, P.; Dalas, E. The Effect of Acetaminophen on the Crystal Growth of Calcium Carbonate. *J. Mater. Sci. Mater. Med.* **2007**, *18* (5), 871−875.
(26) Ukrainczyk, M.; Grebičak, M.; Jerić, I.; Kralj, D. Interactions of Salicylic Acid Derivatives with Calcite Crystals. *J. Colloid Interface Sci.* **2012**, *365* (1), 296−307.
(27) Ukrainczyk, M.; Gredic, M.; Jeric, I.; Kralj, D. Interactions of Scalenohedral Calcite Crystals Withacidic Amino Acid Derivatives of Salicylic Acid. *Cryst. Growth Des.* **2014**, *14*, 4335−4346.
(28) Magnabosco, G.; Giosia, M. D.; Polishchuk, I.; Weber, E.; Fermani, S.; Bottoni, A.; Zerbetto, F.; Pelicci, P. G.; Pokroy, B.; Rapino, S.; Falini, G.; Calvaresi, M. Calcite Single Crystals as Hosts for Atomic-Scale Entrapment and Slow Release of Drugs. *Adv. Healthcare Mater.* **2015**, *4* (10), 1510−1516.
(29) Ukrainczyk, M.; Greiner, M.; Elts, E.; Briesen, H. Simulating Preferential Sorption of Tartrate on Prismatic Calcite Surfaces. *CrystEngComm* **2015**, *17* (1), 149−159.
(30) Borukhin, S.; Bloch, L.; Radlauer, T.; Hill, A. H.; Fitch, A. N.; Pokroy, B. Screening the Incorporation of Amino Acids into an Inorganic Crystalline Host: The Case of Calcite. *Adv. Funct. Mater.* **2012**, *22* (20), 4216−4224.
(31) Malkaj, P.; Dalas, E. Calcium Carbonate Crystallization in the Presence of Aspartic Acid. *Cryst. Growth Des.* **2004**, *4* (4), 721−723.
(32) Nada, H. Difference in the Conformation and Dynamics of Aspartic Acid on the Flat Regions, Step Edges, and Kinks of a Calcite Surface: A Molecular Dynamics Study. *J. Phys. Chem. C* **2014**, *118* (26), 14335−14345.
(33) Green, D. C.; Ihli, J.; Kim, Y. Y.; Chong, S. Y.; Lee, P. A.; Empson, C. J.; Meldrum, F. C. Rapid Screening of Calcium Carbonate Precipitation in the Presence of Amino Acids: Kinetics, Structure, and Composition. *Cryst. Growth Des.* **2016**, *16* (9), 5174−5183.
(34) Kim, Y.; Carloni, J. D.; Demarchi, B.; Sparks, D.; Reid, D. G.; Kunitake, M. E.; Tang, C. C.; Duer, M. J.; Freeman, C. L.; Pokroy, B.; Penkman, K.; Harding, J. H.; Estroff, L. A.; Baker, S. P.; Meldrum, F. C. Tuning Hardness in Calcite by Incorporation of Amino Acids. *Nat. Mater.* **2016**, *15*, 903−910.
(35) Štajner, L.; Kontrec, J.; NjegićDžakula, B.; Maltar-Strmečki, N.; Plodinec, M.; Lyons, D. M.; Kralj, D. The Effect of Different Amino Acids on Spontaneous Precipitation of Calcium Carbonate Polymorphs. *J. Cryst. Growth* **2018**, *486*, 71−81.
(36) Fauchere, J. -L.; Charton, M.; Kier, L. B.; Verloop, A.; Pliska, V. Amino Acid Side Chain Parameters for Correlation Studies in Biology and Pharmacology. *Int. J. Pept. Protein Res.* **1988**, *32* (4), 269−278.
(37) Nomoto, A.; Nishinami, S.; Shiraki, K. Solubility Parameters of Amino Acids on Liquid-Liquid Phase Separation and Aggregation of Proteins. *Front. Cell Dev. Biol.* **2021**, *9* (June), 1−7.
(38) Andersen, F. A.; Kralj, D. Determination of the Composition of Calcite-Vaterite Mixtures by Infrared Spectrophotometry. *Appl. Spectrosc.* **1991**, *45* (10), 1748−1751.
(39) Brečević, L.; Kralj, D. Kinetics and Mechanisms of Crystal Growth in Aqueous Systems. In *Interfacial dynamics*; Mercel Dekker: New York, 2000; pp 435−474.
(40) Sangwal, K. *Additives and Crystallization Processes*; John Wiley & Sons Ltd: Chichester, 2007.
(41) Kubota, N.; Mullin, J. W. A Kinetic Model for Crystal Growth from Aqueous Solution in the Presence of Impurity. *J. Cryst. Growth* **1995**, *152* (3), 203−208.
(42) Sangwal, K. Kinetic Effects of Impurities on the Growth of Single Crystals from Solutions. *J. Cryst. Growth* **1999**, *203* (1), 197−212.
(43) Churchill, H.; Teng, H.; Hazen, R. M. Correlation of PH-Dependent Surface Interaction Forces to Amino Acid Adsorption: Implications for the Origin of Life. *Am. Mineral.* **2004**, *89* (7), 1048−1055.
(44) Stepić, R.; Jurković, L.; Klementyeva, K.; Ukrainczyk, M.; Grebičak, M.; Smith, D. M.; Kralj, D.; Smith, A. S. Adsorption of Aspartate Derivatives to Calcite Surfaces in Aqueous Environment. *Cryst. Growth Des.* **2020**, *20* (5), 2853−2859.
(45) Geffroy, C.; Foissy, A.; Persello, J.; Cabane, B. Surface Complexation of Calcite by Carboxylates in Water. *J. Colloid Interface Sci.* **1999**, *211* (1), 45−53.
(46) Brkljača, Z. *Application of Computational Methods to the Structural and Functional Properties of Flexible Chiral Molecules*; Doktorski rad, Naturwissenschaftlichen Fakultät: Friedrich-Alexander Universität Erlangen-Nürnberg, 2016.
(47) Orme, C. A.; Noy, A.; Wierzbicki, A.; McBride, M. T.; Grantham, M.; Teng, H. H.; Dove, P. M.; De Yoreo, J. J. Formation of Chiral Morphologies through Selective Binding of Amino Acids to Calcite Surface Steps. *Nature* **2001**, *411* (81), 775−779.
(48) Ning, Y.; Meldrum, F. C.; Armes, S. P. Efficient Occlusion of Oil Droplets within Calcite Crystals. *Chem. Sci.* **2019**, *10*, 8964−8972.
(49) Ning, Y.; Han, L.; Derry, M. J.; Meldrum, F. C.; Armes, S. P. Model Anionic Block Copolymer Vesicles Provide Important Design Rules for Efficient Nanoparticle Occlusion within Calcite. *J. Am. Chem. Soc.* **2019**, *141*, 2557−2567.
(50) Ning, Y.; Han, Y.; Han, L.; Derry, M. J.; Armes, S. P. Exerting Spatial Control During Nanoparticle Occlusion within Calcite Crystals. *Angew. Chem., Int. Ed.* **2020**, *59*, 17966−17973.

https://doi.org/10.1021/acsomega.5c13043
ACS Omega 2026, 11, 14002−14016